A simple linearization method unveils hidden enzymatic assay interferences

Maria Filipa Pinto[a,b,c,d], Jorge Ripoll-Rozada[c,d], Helena Ramos[e], Emma E. Watson[f],
Charlotte Franck[f], Richard J. Payne[f], Lucília Saraiva[e], Pedro José Barbosa Pereira[c,d],
Annalisa Pastore[g], Fernando Rocha[b], Pedro M. Martins[a,c,d,*]

[a] Instituto de Ciências Biomédicas Abel Salazar (ICBAS), Universidade do Porto, Porto, Portugal
[b] Laboratório de Engenharia de Processos, Ambiente, Biotecnologia e Energia (LEPABE), Faculdade de Engenharia da Universidade do Porto (FEUP), Porto, Portugal
[c] IBMC - Instituto de Biologia Molecular e Celular, Universidade do Porto, Porto, Portugal
[d] Instituto de Investigação e Inovação em Saúde, Universidade do Porto, Porto, Portugal
[e] Laboratório Associado para a Química Verde (LAQV), Rede de Química e Tecnologia (REQUIMTE), Faculdade de Farmácia da Universidade do Porto (FFUP), Porto, Portugal
[f] School of Chemistry, The University of Sydney, Sydney, New South Wales 2006, Australia
[g] Maurice Wohl Clinical Neuroscience Institute, King's College London, London, England, UK

HIGHLIGHTS

- Kinetic analysis of progress curves is shown to reveal enzymatic assay interferences.
- The new linearization method (LM) requires no additional experiments to be applied.
- The LM can be routinely used as a stringent quality check of enzymatic assays.
- Real case-studies are presented to illustrate the applicability of the new method.
- This tool is expected to increase the reproducibility of enzymology data.

GRAPHICAL ABSTRACT
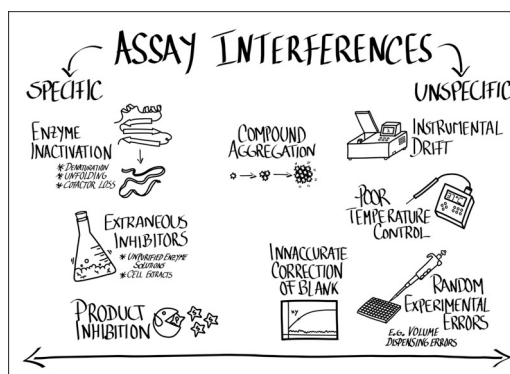
ABSTRACT

Enzymes are among the most important drug targets in the pharmaceutical industry. The bioassays used to screen enzyme modulators can be affected by unaccounted interferences such as time-dependent inactivation and inhibition effects. Using procaspase-3, caspase-3, and α-thrombin as model enzymes, we show that some of these effects are not eliminated by merely ignoring the reaction phases that follow initial-rate measurements. We thus propose a linearization method (LM) for detecting spurious changes of enzymatic activity based on the representation of progress curves in modified coordinates. This method is highly sensitive to signal readout distortions, thereby allowing rigorous selection of valid kinetic data. The method allows the detection of assay interferences even when their occurrence is not suspected *a priori*. By knowing the assets and liabilities of the bioassay, enzymology results can be reported with enhanced reproducibility and accuracy. Critical analysis of full progress curves is expected to help discriminating experimental artifacts from true mechanisms of enzymatic inhibition.

1. Introduction

Typically, more than one-third of the discrete drug targets in the portfolio of pharmaceutical companies consists of enzymes [1], with phosphate-transferring enzymes, or kinases, being the largest category of potentially novel drug targets [2]. Drug screening is usually based on enzymatic assays that aim at identifying compounds that inhibit, enhance or modulate enzyme activity. However, the output of these assays strongly depends on the experimental conditions and on several different parameters that are often difficult to master completely. In high-throughput screening (HTS) of enzyme modulators, primary assays employing light-based detection methods are escorted by orthogonal assays using different output reporters in order to identify false positives and fluorescence/luminescence artifacts [3,4]. Other possible interferences can be specific of a given system, such as the occurrence of enzyme inactivation and competitive product inhibition, or unspecific, as in the cases of random experimental errors and of changes in experimental parameters during the reaction (Fig. 1). This uncertainty dramatically calls for new and more sensitive approaches to allow fast and reliable detection of these interferences.

While no kinetic method is currently available to detect generic interferences in enzymatic assays, in the specific case of enzyme inactivation interferences their occurrence can be detected by the Selwyn test applied to progress curves measured at different enzyme concentrations (E_0) and constant substrate concentration (S_0) [12]. Yet, besides requiring the realization of additional experiments, the Selwyn test provides no quantitative information of inactivation rates [13] and might not detect incomplete enzyme inactivation. In the case of nonspecific aggregation interferences in HTS assays, counter-screens of β-lactamase inhibition in the presence and absence of detergent are performed to check for the presence of promiscuous inhibitors [14]. In the present contribution, we propose a touchstone criterion for the detection of assay interferences based on the graphical representation
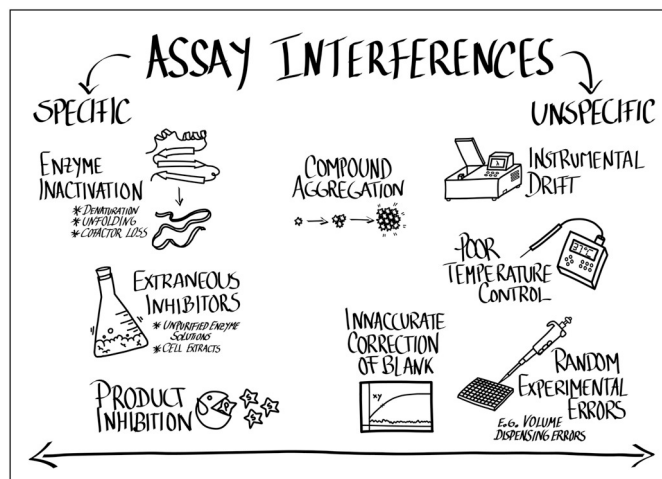
Fig. 1. Specific and unspecific interferences on enzymatic assays. Spurious effects that are too small to be readily observable can produce important errors of interpretation of kinetic results. Specific of a given system, enzyme inactivation can be prevented by the addition of protein stabilizers or by increasing the concentration of enzyme [5]. Extraneous inhibitors present in unpurified enzyme solutions or in cell extracts systematically affect the quality of kinetic measurements [6]. Product inhibition can usually be ignored in initial-rate measurements but is highly misleading in time-course studies [7]. Compound aggregation can cause enzyme sequestration on the surface of the aggregate particles and is one of the main reasons for promiscuous enzyme inhibition [3,8]. Instrumental drift, poor temperature control, inaccurate correction of the sample blank, and random experimental errors in e.g. volume dispensing operations are typical examples of unspecific interferences [9,10]. Adequate buffering of the reaction mixture is important to prevent changes of enzyme activity provoked by drifts in pH and ionic strength [11].

of reaction coordinates in a linearized scale. We applied our method to enzymatic reactions catalyzed by procaspase-3, caspase-3 (EC 3.4.22.56) and α-thrombin (EC 3.4.21.5). Caspases are a family of cysteine-dependent aspartate-specific peptidases (MEROPS family C14; [15]) synthesized as zymogens and converted into their more active forms upon proteolytic cleavage [16]. Both caspase-3 and its precursor procaspase-3 undergo progressive inactivation during *in vitro* enzymatic assays. Progress curves of procaspase-3- and caspase-3-catalyzed reactions are analyzed to identify enzyme inactivation and characterize its relative importance. Alpha-thrombin is a (chymo)trypsin-like serine peptidase (MEROPS family S01; [15]) and a main effector in the coagulation cascade. Similar to caspase-3, its zymogen (prothrombin) is cleaved to generate the active form of the enzyme. Thrombin generation is tightly regulated to allow blood clot formation after an injury [17]. A variety of thrombin-targeting inhibitors is produced by blood-feeding organisms [18–21]. The outcome of the new test in the presence of enzyme inhibition is demonstrated for α-thrombin-catalyzed reactions inhibited by a synthetic variant of an anticoagulant produced by *Dermacentor andersoni* [22,23]. Along with the inactivation and inhibition studies, we discuss the detection of unspecific interferences arising from changes in the reaction conditions.

2. Experimental procedures

2.1. Procaspase-3 production in yeast cell extracts

Procaspase-3 was produced as previously described [24,25]. Briefly, cultures of *Saccharomyces cerevisiae* transformed with the expression vector pGALL-(*LEU2*) encoding human procaspase-3 were diluted to 0.05 optical density at 600 nm (OD_{600}) in 2% (w/v) galactose selective medium and grown at 30 °C with continuous shaking until an OD_{600} range of 0.35–0.40. Cells were collected by centrifugation and frozen at −80 °C. For protein extraction, cell pellets were thawed, treated with *Arthrobacter luteus* lyticase (Sigma-Aldrich, Sintra, Portugal), and the cells were lysed using CelLytic™ Y Cell Lysis Reagent (Sigma-Aldrich, Sintra, Portugal) in the presence of 1 mM phenylmethylsulfonyl fluoride, 1 mM Dithiothreitol (DTT), 1 mM ethylenediaminetetraacetic acid (EDTA), 0.01% (v/v) Triton X-100. Total protein concentration of the extracts was determined using the Pierce™ Coomassie Protein Assay Kit (ThermoFisher Scientific, Porto Salvo, Portugal).

2.2. Enzymatic assays for procaspase-3 and caspase-3

The activity of recombinant human procaspase-3 (STRENDA ID 1XV0MK) and of recombinant human purified caspase-3 (STRENDA ID M9FKPY) was followed by monitoring the conversion of the fluorogenic substrate Acetyl-Asp-Glu-Val-Asp-7-amido-4-methylcoumarin (Ac-DEVD-AMC, Sigma-Aldrich, Sintra, Portugal) to 7-amino-4-methylcoumarin (AMC) at 37 °C. Procaspase-3 (0.123 mg/mL protein extract) and caspase-3 (1.0 U, Enzo Life Sciences, Lisboa, Portugal) were assayed in 96-well microplates (Nunc™ MicroWell™ 96-Well, Thermo Scientific™, ThermoFisher Scientific, Porto Salvo, Portugal) using 100 μL of 20 mM HEPES pH 7.4 (20 °C), 100 mM NaCl, 10% (w/v) sucrose, 0.1% (w/v) CHAPS, 10 mM DTT, 1 mM EDTA per well [26]. A range of substrate concentrations of 3.125–300 μM Ac-DEVD-AMC for procaspase-3, and 3.125–50 μM Ac-DEVD-AMC for caspase-3 were tested. The reactions were started by addition of protein, and fluorescence was monitored at 460 nm (390 nm excitation) using a HIDEX CHAMELEON V plate reader (Turku, Finland). To avoid evaporation, the reaction mixture in each well was overlaid with liquid paraffin (100 μL). All solutions were equilibrated to 37 °C before use. Assays were performed in triplicate or quadruplicate for procaspase-3, and in duplicate for purified caspase-3. The calibration curve was built using solutions with known concentration of the free fluorescent product AMC (Sigma-Aldrich, Sintra, Portugal).

2.3. Enzymatic assay for α-thrombin

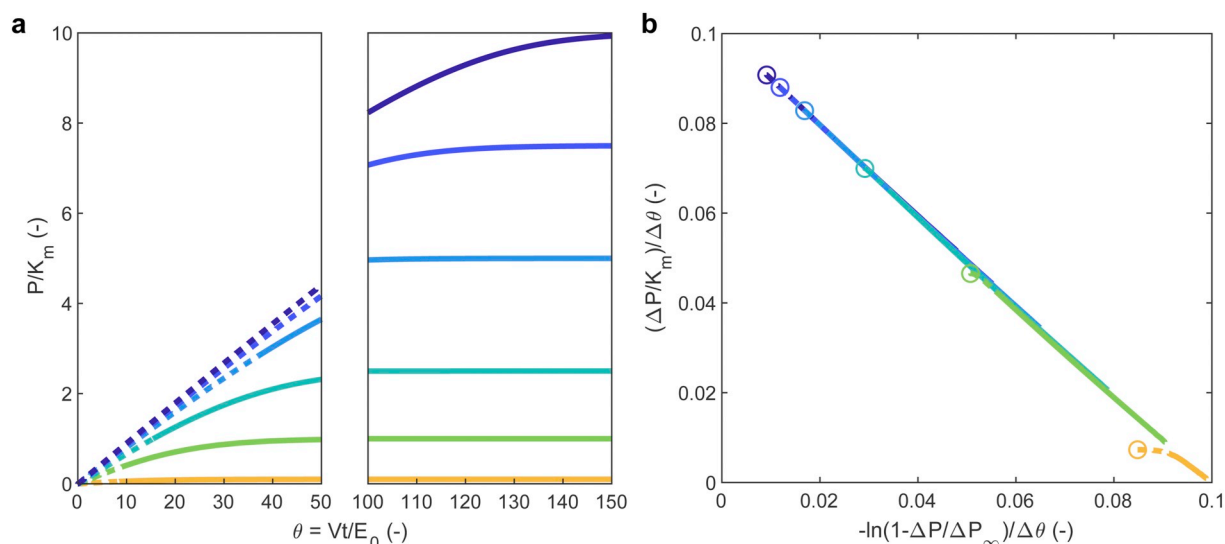The enzymatic activity of human α-thrombin (0.15 nM, Haematologic Technologies, Essex, USA) was assessed by following its amidolytic activity toward the chromogenic substrate Tos-Gly-Pro-Arg-p-nitroanilide (25–400 μM, Chromozym TH, Roche, Amadora, Portugal) at 37 °C in the presence of 0.40 nM of a synthetic variant of an anticoagulant produced by *D. andersoni* [23] - STRENDA ID OUYDF2. The assays were performed at least in duplicate in 200 μL of 50 mM Tris pH 8.0 (20 °C), 50 mM NaCl, 1 mg/mL BSA. The reactions were initiated by the addition of α-thrombin and followed at 405 nm using a Synergy2 multi-mode microplate reader (BioTek Winooski, USA) [27].

3. The linearization method

Deviations from the normal progress of enzyme-catalyzed reactions should, in principle, alter the build-up profile of product concentration (P) vs. time (t) from the theoretical curve expected by the integrated form of the Michaelis-Menten (MM) equation [28–30]:

$$P = Vt + K_m \ln\left(1 - \frac{P}{S_0}\right) \tag{1}$$

where S_0 is the initial substrate concentration and K_m and V are the Michaelis constant and the limiting rate, respectively. In practice, however, Eq. (1) is not used to detect assay interferences since no evident changes in the shape of the progress curves are induced by enzyme inactivation, product inhibition, and quasi-equilibrium mechanisms of competitive inhibition, uncompetitive inhibition, etc. [31]. Eq. (1), which in its closed-form version is also known as the Schnell-Mendoza equation [28], produces poorer estimates of kinetic parameters than the classic MM equation fitted to initial reaction rate measurements because any external interference may severely accumulate over the full time-course [29,30]. In addition, the application of Eq. (1) is limited to a range of conditions more restricted than that of $E_0 \ll S_0 + K_m$ required to validate the steady-state assumption [32,33]: Eq. (1) fails to account for the fast transient phase that precedes the steady-state phase according to the closed-form solution of the Briggs-Haldane reaction mechanism (Fig. 2a). Additionally, the effect of E_0 can be masked by apparent values of the Michaelis constant ($K_m^{app} \approx K_m + E_0$), especially for $E_0 \geq K_m$ [34].

We propose a new linearization method (LM) for the detection of assay interferences based on the following modified version of the integrated MM equation:

$$\frac{\Delta P}{\Delta t} = V^{app} - \left[-K_m^{app} \ln\left(1 - \frac{\Delta P}{\Delta P_\infty}\right)\middle/ \Delta t\right] \tag{2}$$
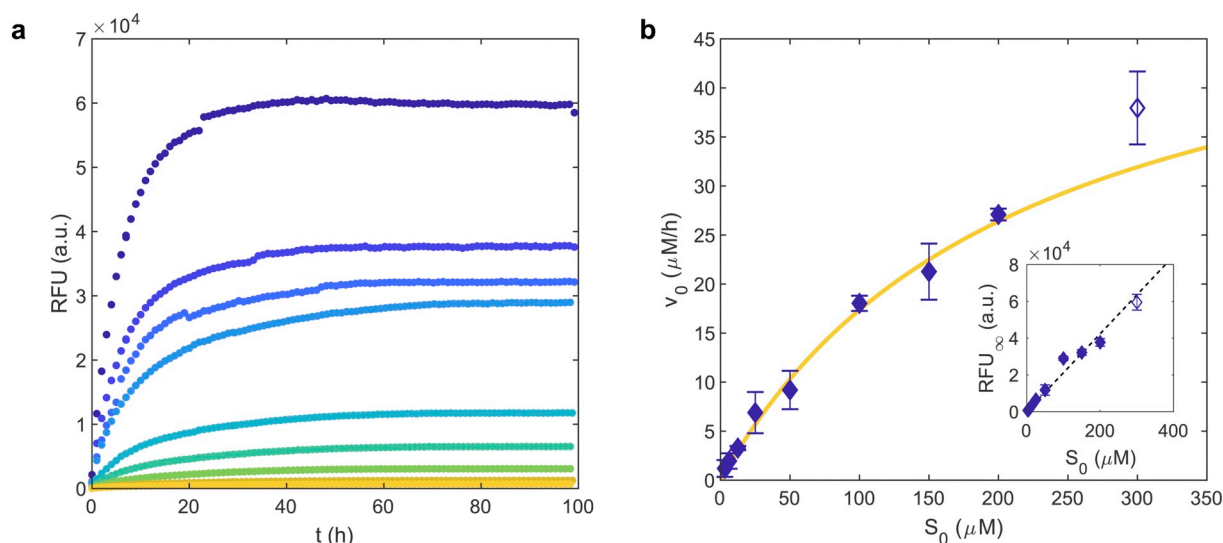
The main differences of this formalism relatively to Eq. (1) are: (a) the use of apparent kinetic constants K_m^{app} and V^{app}, (b) the use of partial time intervals ($\Delta t = t - t_i$) and of the corresponding increment of product concentration ($\Delta P = P - P_i$), (c) the initial condition (subscript i) is now any point of the reaction subsequent to the pre-steady-state phase ($t_i > t^*$), (d) the final concentration of product is given by the measured value (P_∞) and not by the expected value (S_0) [30], and (e) Eq. (2) is presented in a linearized form of the Walker and Schmidt type [35] (Fig. 2b). Features (a) to (c) are meant to expand the validity of time-course analysis to the same range of conditions of the steady-state assumption ($E_0 \ll S_0 + K_m$) [34,36]. Feature (d) takes into account possible discrepancies between P_∞ and S_0 values resulting, for example, from complete enzyme inactivation or inaccurate pipetting. Feature (e) is implemented because the Walker and Schmidt linearization [35] is highly sensitive to fluctuations in P readouts [37], whereas linearity is an easily implementable judgment criterion.

The linear variation of $\Delta P/\Delta t$ with $-\ln(1 - \Delta P/\Delta P_\infty)/\Delta t$ expected by Eq. (2) is a necessary but not sufficient condition to reject assay interferences. To pass this test, the straight lines obtained at different substrate concentrations should also superimpose (Fig. 2b). Although parameter estimation is not the primary goal here, the agreement between the apparent constants and the values of K_m and V obtained by the standard initial-rate method further confirms that the assay is unbiased. Finally, since the LM equation applies to single active site, single substrate and irreversible steady-state reactions of the Briggs-Haldane type [38], this method might also be used to reveal the presence of a more complex enzymatic mechanism from the one assumed.

4. Results and discussion

4.1. Procaspase-3 inactivation - preliminary analysis

The exponential reaction curves of Ac-DEVD-AMC cleavage by procaspase-3 (Fig. 3a) are not suggestive of any evident loss of enzyme

Fig. 2. Theoretical progress curves expected for unbiased Briggs-Haldane reaction mechanisms. (a) Evolution of product concentration over time represented in dimensionless units of product concentration ($p = P/K_m$) and time ($\theta = Vt/E_0$) for different substrate concentrations. Different colors correspond to values of $s_0 = S_0/K_m$ of (from top to bottom) 10, 7.5, 5, 2.5, 1, 0.1 (additional simulation parameters given in Table A1, Appendix). The broken x axis is used to emphasize the initial periods of constant velocity (dashed lines). (b) The same curves are represented in linearized coordinates according to Eq. (2); round markers indicate the steady-state instant t^*. The absence of assay interferences is evidenced by negatively-sloped, superimposing straight lines.

Fig. 3. Loss of procaspase-3 activity is not self-evident in a first analysis of kinetic results. (a) Fluorescence (*RFU*) increase during the cleavage of Ac-DEVD-AMC by procaspase-3 for S_0 values of (from top to bottom) 300, 200, 150, 100, 50, 25, 12.5, 6.25, and 3.125 μM. (b) Plot of the initial reaction rates (v_0) as a function of substrate concentration. Symbols and error bars: means and standard deviations of v_0 values calculated using the initial slopes obtained in (a) and a preliminary calibration curve relating the end-point fluorescence (RFU_∞) and S_0 (inset). Solid line: fit of the MM equation to selected experimental data (closed symbols). Since the results are affected by severe enzyme inactivation, the fitted values of $K_m = 217 \pm 59$ μM and $V = 55 \pm 9$ μM/h ($R^2 = 0.9919$) are merely indicative. Inset: linear fit (dashed line) to selected (closed symbols) RFU_∞ vs. S_0 data ($R^2 = 0.9532$).

activity over time. The lack of well-defined slopes from which the initial rates (v_0) can be accurately measured might only indicate that the substrate concentrations are still too low to achieve the saturating MM conditions [39,40]. In fact, the plateau corresponding to V in the MM representation (Fig. 3b) is barely noticeable in the studied range of substrate concentrations.

The obtained value of $K_m = 217 \pm 59$ μM is 62-fold higher than that previously reported using the uncleavable mutant procaspase-3(D_3A), which has three processing sites removed, and the substrate Ac-DEVD-AFC, which has a different fluorescent reporter (AFC) than Ac-DEVD-AMC [41]. Differences between the observed and the literature values of K_m could therefore be ascribed to the distinct nature of each enzymatic assay. Yet, the calibration curve represented in Fig. 3b (inset) provides important clues as to the possible existence of experimental artifacts. This is a conditional calibration curve since the final fluorescence value (RFU_∞) is assumed to result from a complete catalytic reaction in which the final product concentration P_∞ is equivalent to S_0. To check the validity of this hypothesis, reference fluorophore solutions were used to calibrate the equipment according to the standard protocol (Fig. 4a); for the same concentrations of fluorophore and substrate, the fluorescence intensity of the calibration solutions (RFU_{cal}) clearly surpasses the RFU_∞ signal, thus suggesting partial conversion of substrate into products during the reactions (Fig. 3a). This finding invalidates the preliminary calibration curve and the kinetic analysis in Fig. 3b since the condition of complete chemical reaction is not observed. Whether or not the reactions were really unfinished and what were the mechanisms thereby involved cannot be ascertained by the calibration-curve test alone. Besides procaspase-3 inactivation, other interfering factors, such as fluorescence quenching phenomena, could have caused the observed differences between RFU_{cal} and RFU_∞. The occurrence of progressive loss of enzyme activity was further confirmed by the Selwyn test (Fig. 4b) and by the direct measurement of procaspase-3 activity for different periods of incubation in the reaction environment (Fig. 4c). Relatively to these methods, the calibration-curve test (Fig. 4a) has the advantage of requiring no other experiments than those already performed while estimating MM kinetic parameters. Furthermore, if enzyme inactivation is admitted as a first-order decay

process, the following relationship can be used to quantitatively estimate the product of the decay rate constant λ by the time constant $\tau = K_m/V$ (Appendix):

$$P_\infty = S_0 - K_m \omega \left[\frac{S_0}{K_m} \exp\left(\frac{S_0}{K_m} - \frac{1}{\tau\lambda} \right) \right] \tag{3}$$

For a given substrate concentration, the extent of the reaction is ultimately determined by the product $\tau\lambda$ relating the rates of inactivation and of unimpaired reaction. It follows from the inverse dependence of $\tau\lambda$ on E_0 (via τ and V) that the effects of inactivation can be counterbalanced by increasing the concentration of enzyme. Similar improvements can be achieved by decreasing the value of λ through the use of protein stabilizers. The fitted value of $\tau\lambda = 1.4 \pm 0.3$ is clearly in the region above ~0.1 for which complete enzyme inactivation can be attained before the conversion of the total available substrate (view Tables A2 and A3). Contrary to the estimation obtained by initial-rate analysis, the fitted value of $K_m = 161 \pm 77$ μM is obtained taking into account the effect of enzyme inactivation. The quantitative information provided by the calibration-curve test is an advantage over the Selwyn test, whose underlying principle also requires additional progress curves to be measured with various enzyme concentrations and constant S_0 values [12]. In the case described in Fig. 4b, the non-superimposed Selwyn plots of P against E_0t confirm the likely occurrence of procaspase-3 inactivation, as previously suggested by simple inspection of the calibration curves (Fig. 4a). The last evidence supporting the verdict of both tests is obtained by directly measuring the enzymatic activity at the end of different periods of incubation in the reaction environment (Fig. 4c). Procaspase-3 activity is confirmed to rapidly decrease with time according to the exponential decay trend expected for first-order processes. The reciprocal of the decay rate constant ($1/\lambda = 8.3$ h) can be interpreted as the period of time required for the catalytic activity to drop to ~37% of its initial value.

4.2. Loss of procaspase-3 activity identified by the linearization method

Complete catalytic reactions, promoted for example by high E_0 values or by low S_0 values, can pass the calibration-curve and the Selwyn
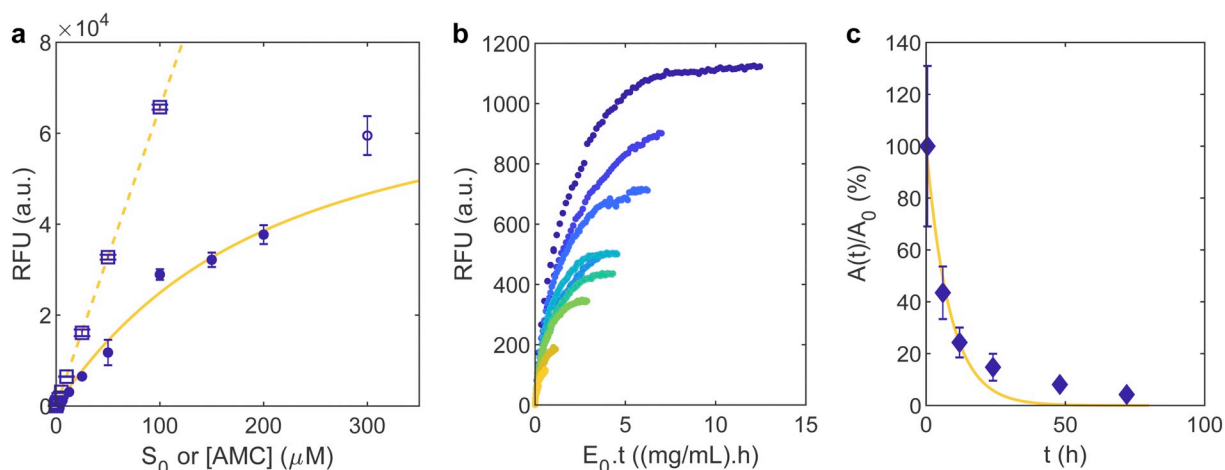
Fig. 4. Procaspase-3 inactivation identified by different methods. (a) The calibration-curve test is proposed based on the differences between *expected* (RFU_{cal}, squares) and *obtained* (RFU_{∞}, circles) end-point signals. Symbols and error bars represent means and standard deviations. The values of RFU_{cal} are measured using solutions of known fluorophore concentrations ([AMC]). The test passes if the values of RFU_{cal} and RFU_{∞} superimpose. Solid line: Eq. (3) is fitted to the experimental data (fitting results: $K_m = 161 \pm 77$ μM and $\tau\lambda = 1.4 \pm 0.3$ h, $R^2 = 0.9851$). The obtained end-point signals are the same used to build the preliminary calibration curve in the inset of Fig. 3b. Dashed line: linear fit representing the true calibration curve ($R^2 = 1$). (b) The classic Selwyn test also suggests time-dependent loss of procaspase-3 activity since progress curves measured for (from top to bottom) 0.17, 0.13, 0.09, 0.06, 0.07, 0.06, 0.04, 0.02, 0.01 mg/mL procaspase-3 and constant S_0 (3.125 μM) are not superimposable when represented in a modified $E_0 t$ timescale [12]. (c) Symbols and error bars: means and standard deviations of the normalized enzymatic activity $A(t)/A_0$ after different periods of incubation. Solid line: numerical fit to an exponential decay function (fitted result: $\lambda = 0.12 \pm 0.02$ h^{-1}, $R^2 = 0.9655$).
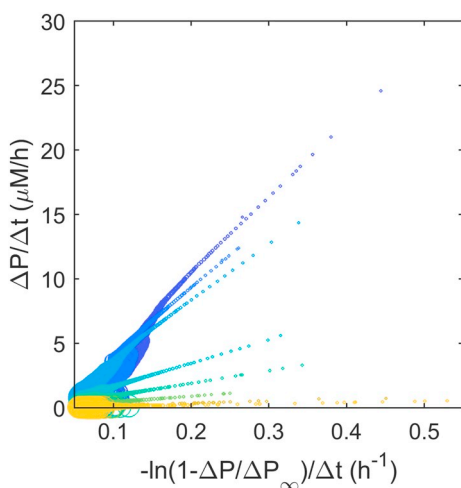
Fig. 5. Using the LM test to detect procaspase-3 inactivation. The progress curves in Fig. 3a measured for S_0 values of 200, 150, 100, 50, 25, 12.5, 6.25, and 3.125 μM are now represented in the linearized $\Delta P/\Delta t$ vs. $-\ln(1 - \Delta P/\Delta P_{\infty})/\Delta t$ scale (color-coded as in Fig. 3a). Symbol size increases with the time-course of the reaction. Non-superimposing, positively-sloped straight lines clearly indicate the occurrence of assay interferences, which, in the present case, are associated with procaspase-3 inactivation (Fig. 4).

tests even in presence of significant enzyme inactivation. This misjudgment may affect the overall quality of reported enzymology data, particularly when the initial reaction rate phase is itself difficult to define, as in conditions of $S_0 < K_m$ [39,42]. Enhanced limits of detection to this and other interferences can be achieved by application of the new LM test brought forward by Eq. (2). In the commonest case of $E_0 \ll K_m$, the intervals Δt and ΔP can be considered right from the beginning of the measurements because the steady-state condition starts to be valid after the first milliseconds of the reaction [34,43]. The non-conformity of the linearized curves of procaspase-3 (Fig. 5) with the

ideal behavior previously described in Fig. 2b is evident: the linearized progress curves obtained for different values of S_0 show positive slopes (rather than negative slopes) and do not superimpose.

The calibration-curve test, the Selwyn test and the LM test are all capable of detecting the progressive inactivation of procaspase-3. For practical uses, the new methods here proposed are more easily applicable than having to prearrange and perform additional Selwyn test experiments. However, the question remains open as to which of the three methods is more sensitive to slight losses of enzymatic activity. In order to study milder decay processes than that observed for procaspase-3 in cell extracts, values of $\tau\lambda < 1.4$ were used in the numeric simulations described in detail in the Appendix (Tables A2–A4). For a reference value of $\tau\lambda = 0.1$ and assuming S_0/K_M ratios between ~1 and ~5, both the calibration-curve test (Fig. 6a) and the Selwyn test (Fig. 6b) fail to reveal S_0-dependent effects caused by inactivation. Conversely, these effects are visibly amplified in Fig. 6c where the ($\Delta P/K_m$)/$\Delta\theta$ vs. $-\ln(1 - \Delta P/\Delta P_{\infty})/\Delta\theta$ curves are at once non-linear and non-superimposing. Therefore, our experimental and numeric results confirm that the LM test is a practical, yet stringent, alternative to detect enzyme inactivation.

### 4.3. Unspecific interferences detected in the caspase-3 assay

Faster catalytic reactions are expectable for purified caspase-3 relatively to procaspase-3, which, besides being less active, is present in low concentration in cell extracts. Consequently, the inactivation issues considered for the proenzyme are less important for the purified enzyme - note that the duration of the enzymatic reactions decreases from > 1 day (Fig. 3a) to < 1 h (Fig. 7a). New challenges for the accurate determination of kinetic parameters are, however, posed by the shorter reaction timescales. This is illustrated in Fig. 7a, where the phase of constant velocity is not clearly defined during a stabilization period of ~10 min. Short periods of normalization of reaction conditions are hardly avoidable even when, as in the present case, the component solutions are pre-equilibrated to the reaction temperature, or when miniaturized high-throughput devices are employed [44]. Small temperature variations markedly influence enzymatic reaction
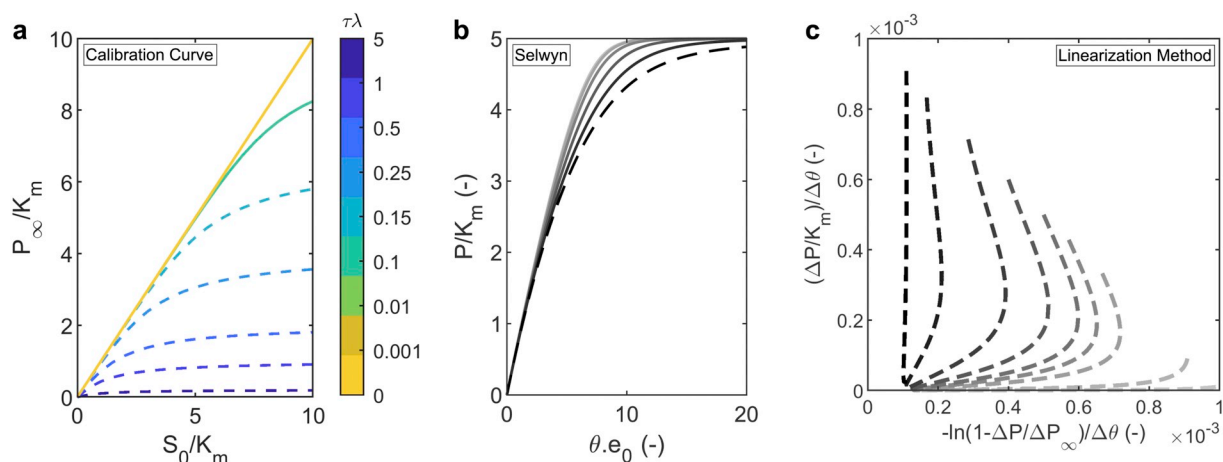
Fig. 6. The LM test is highly sensitive to enzyme inactivation. Detection limits of the (a) calibration-curve test, (b) Selwyn test and (c) the LM test according to the theoretical progress curves simulated assuming a first-order decay of enzyme activity (simulation parameters listed in Tables A2–A4). Dashed and solid lines: cases of successful and failed detection, respectively. (a) The calibration-curve test fails to detect inactivation for $\tau\lambda$ values (color bar) below 0.1, as the measurable and expected values of final product concentration (P_∞ and S_0) start to be undistinguishable. (b) Theoretical progress curves simulated for varying e_0 values for a range of $\tau\lambda$ values between 10^{-3} and 0.1 (from lighter to darker shades of gray), and $S_0/K_m = 5$. The Selwyn test fails to detect inactivation for $\tau\lambda < 0.1$, as the Selwyn curves are not easily distinguishable. (c) Theoretical LM curves simulated for a reference value of $\tau\lambda = 0.1$ and a range of S_0/K_m values between (from lighter to darker shades of gray) 0.1 and 10. This test detects inactivation under conditions of $\tau\lambda = 0.1$ and $S_0/K_m < 5$ for which the calibration-curve test and the Selwyn test have poor sensitivity.

rates and in a S_0-dependent manner [45]. After confirming that the caspase-3 assay is not affected by significant enzyme inactivation (Fig. 7b) the reaction phases that succeed the first ~10 min interval can be analyzed in detail. Because the initial slopes (and the corresponding values of v_0) are probably affected by drifts in the reaction properties,

instantaneous rates (v_i) obtained upon condition stabilization may be used in v vs S_0 plots as an approximation to the real value of v_0 (Fig. 7c). For rapidly progressing reactions, this procedure raises the doubt of whether the instantaneous substrate concentration is too depleted relative to the initial value (S_0) [46]. Also, it is not granted that the
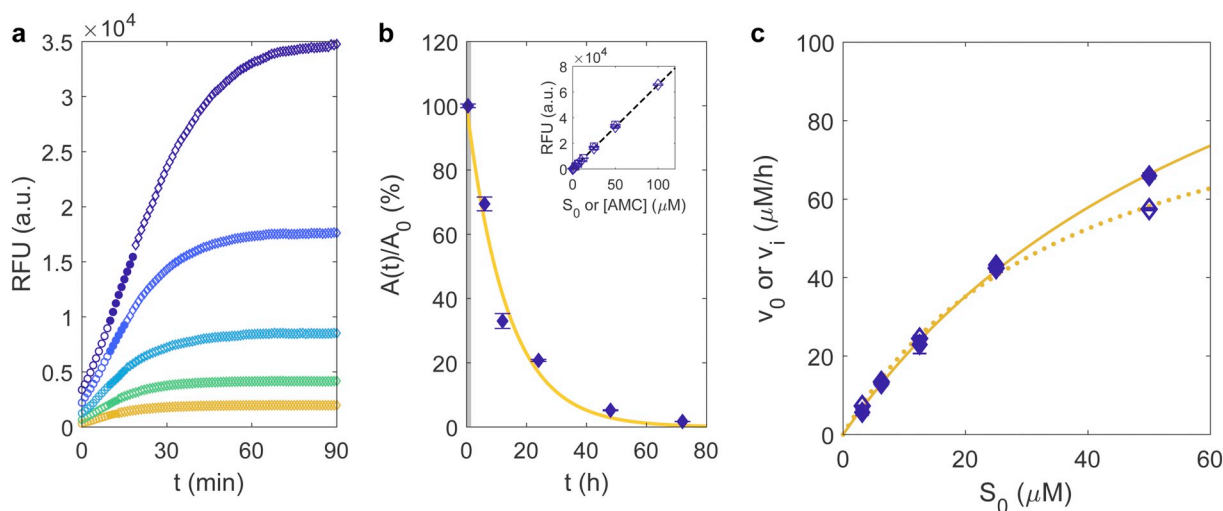
Fig. 7. Assay interferences other than enzyme inactivation may affect the initial-rate measurements in the reactions catalyzed by purified caspase-3. (a) Fluorescence increase during the hydrolysis of Ac-DEVD-AMC by 1.0 U of caspase-3 for S_0 values of (from top to bottom) 50, 25, 12.5, 6.125, and 3.125 μM. Circles: data selected for the determination of initial (open symbols) and instantaneous (closed symbols) slopes. (b) Symbols and error bars: means and standard deviations of direct measurements of caspase-3 activity after different periods of incubation in the reaction environment. No significant inactivation occurs within the full reaction timescale (gray area) considered in (a). Line: Numerical fit to an exponential decay function ($\lambda = 0.074 \pm 0.009$ h^{-1}, $R^2 = 0.9829$). Inset: the calibration-curve test confirms the absence of significant enzyme inactivation: the obtained end-point signals (circles) overlie the calibration curve (dashed line) built with fluorescence measurements of standard AMC solutions (squares). (c) Plot of the initial (v_0) and instantaneous (v_i) reaction rates as a function of the initial substrate concentration (S_0). The experimental values of v_0 (open symbols) and v_i (closed symbols) are calculated using initial and instantaneous slopes, respectively, as represented in (a). Lines: fit of the MM-like equation to the experimental data. Since both v_0 and v_i are imperfect estimations of the initial rate value (see text for details) the fitted values of $K_m = 38.7 \pm 6.4$ μM and $V = 103 \pm 10$ μM/h (dotted line, open symbols, $R^2 = 0.9971$) and $K_m = 71.9 \pm 13.0$ μM and $V = 162 \pm 20$ μM/h (solid line, closed symbols, $R^2 = 0.9982$) are merely indicative.
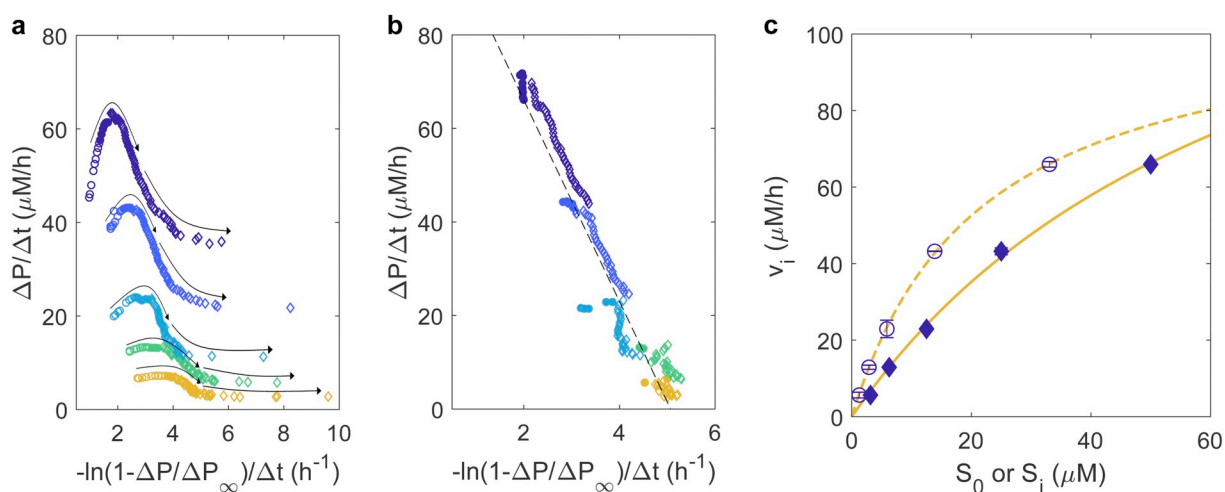
Fig. 8. Time-wise variations in solution properties are detected by the LM test. (a) Symbols: progress curves of Ac-DEVD-AMC catalysis by 1.0 U caspase-3 represented in the linearized scale using $t_i = 0$ min (color-coded as in Fig. 7a). Arrows: visual reference indicating the reaction time-course. The initial experimental outliers (open circles) show up detached from the negatively-sloped trends. The final scattering of the data results from the amplification of random errors and instrumental noise. (b) Symbols: linearized progress curves obtained after discarding the initial outlier points ($t_i = 10$ min). For clarity, only data corresponding to 95% reaction completion are represented. Dashed line: representation of Eq. (2) after replacing K_m^{app} and V^{app} by the values of K_m and V determined by independent methods in (c). (c) Symbols and error bars: means and standard deviations of the instantaneous reaction rates (v_i) represented as a function of S_0 (closed symbols) and S_i (open symbols). Lines: numerical adjustment of the MM-like equation. The v_i vs. S_0 data and numerical fit (closed symbols and solid line) are the same as in Fig. 7c (shown here as visual reference). Dashed line: numerical fit of the v_i vs. S_i data; the fitted results ($K_m = 21.5 \pm 0.9$ μM and $V = 109 \pm 2$ μM/h, $R^2 = 0.9998$) are not affected by major assay interferences as they successfully describe the experimental LM curves in (b).

properties of the reaction mixture are completely stabilized during the period of time over which v_i is determined.

A better perception of the main experimental outliers can be obtained by representing the progress curves in the modified scale proposed by the LM test (Fig. 8a). For each S_0 condition, the initial measurements stand out as evidently separated from the negatively-sloped trend exhibited by most of the subsequent data points. This suggests that the values of v_0 determined from Fig. 7a (open circles) and the resulting kinetic analysis in Fig. 7c (dotted line) are affected by assay interferences. The fact that no straight line common to all S_0 conditions is clearly defined by the late data points does not have a particular meaning because early errors can propagate throughout the $\Delta P/\Delta t$ vs. $-\ln(1 - \Delta P/\Delta P_\infty)/\Delta t$ curve. Moreover, the final amplification of the instrumental noise is expectable in result of the use of the logarithm in the horizontal axis. Setting the new initial condition to $t_i = 10$ min not only eliminates the initial outliers but also improves the quality of the linearized plots (Fig. 8b). The tendency of the different experimental curves to superimpose in a single straight line further confirms that the activity of caspase-3 remains practically unchanged during the time-course of the reactions. Overall, the first (Fig. 8a) and second (Fig. 8b) LM representations validate the enzymatic assay for purified caspase-3, although the initial ~10 min stabilization period should not be considered for analysis. In the determination of instantaneous reaction rates, the used $P(t)$ data (closed circles in Fig. 7a) already integrate the negatively-sloped trends in Fig. 8a. The kinetic laws based on v_i measurements (Fig. 7c, solid line) should, however, take into account the depletion of substrate until the moment when the rate is determined [34]. This correction to the MM plots involves replacing the initial substrate concentration S_0 by the instantaneous substrate concentration S_i, here estimated using median concentration values for the time interval used for v_i determination. The MM parameters fitted to the v_i vs. S_i data (Fig. 8c; $K_m = 21.5$ μM and $V = 109$ μM/h) are considered valid and free from major assay interferences. In accordance to what is expected for steady-state conditions, the apparent kinetic constants K_m^{app} and V^{app} of the LM equation can be approximated by the true

parameters K_m and V. Illustrating this, the experimental LM curves (symbols in Fig. 8b) are well described by the theoretical LM curve computed for $K_m^{app} = K_m$ and $V^{app} = V$ (dashed line in Fig. 8b).

4.4. Inhibition of α-thrombin

The presence of unaccounted enzyme modifiers in the assay solution is another possible interference associated to the use of crude enzyme preparations and cell extracts. The detection of enzyme modulation effects by the LM test is here demonstrated for the inhibition of the amydolytic activity of human α-thrombin by a synthetic variant of an anticoagulant produced by *D. andersoni*. Since the inhibitory effect of subnanomolar concentrations of the enzyme-modifier is known beforehand (Fig. A1, Appendix), the LM test is applied to identify the fingerprints left by enzyme modifiers and to illustrate how cautiously initial-rate measurements should be used during the characterization of inhibition mechanisms.

If (i) quasi-equilibrium conditions are rapidly attained and (ii) the concentration of inhibitor is significantly higher than the concentration of enzyme, progress curves measured in the presence of competitive, uncompetitive or mixed inhibition are still numerically described by Eq. (2), with K_m^{app} and V^{app} being affected by the concentration of inhibitor (s). Consequently, the LM analysis may fail to detect linear inhibition effects provoked by solution contaminants. On the positive side, quasi-equilibrium linear inhibition is a particular case of the general modifier mechanism [47], whose rate equations frequently contain squared concentration terms recognizable as deviations from the LM equation. As such, it is conceivable that the new method can also be used for the preliminary detection of variants of the general modifier mechanism, and not only for assay validation purposes. The complexity of this subject greatly increases as other LM-detectable mechanisms of product inhibition, slow-onset inhibition, substrate competition, allosterism, etc., are considered. Presently, we apply the LM test as a quality-control test to α-thrombin-catalyzed reactions inhibited by a synthetic variant of an anticoagulant produced by *D. andersoni*, and we leave the
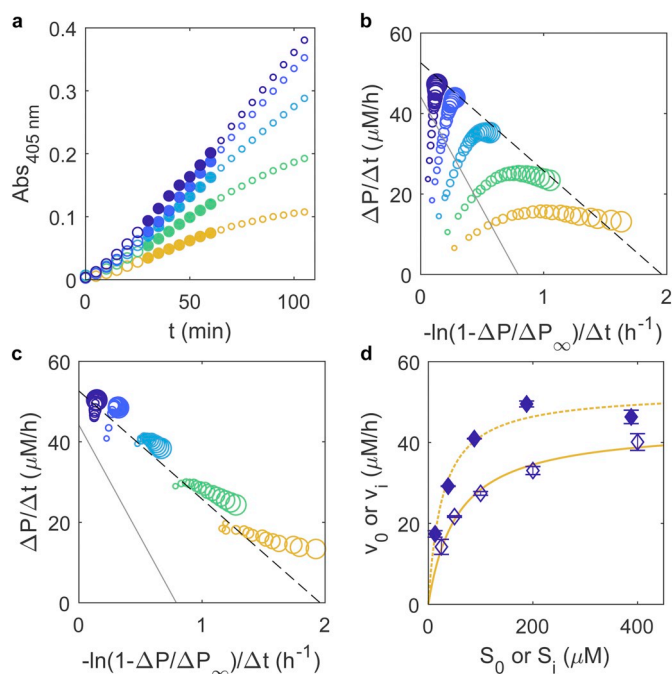
Fig. 9. The LM test detects timewise effects induced by enzyme modifiers. Absorbance (Abs_{405nm}) increase during the catalysis of Tos-Gly-Pro-Arg-pNA by 0.15 nM α-thrombin in the presence of 0.40 nM inhibitor for substrate concentration of (from top to bottom) 400, 200, 100, 50 and 25 μM. Large symbols: data selected for the determination of initial (large open symbols) and instantaneous (closed symbols) slopes. (b) The same progress curves are represented in the linearized scale using $t_i = 0$ min. (c) Symbols: LM progress curves obtained after discarding the initial points ($t_i = 30$ min). (b,c) Lines: representation of Eq. (2) after replacing K_m^{app} and V^{app} by the values of K_m and V determined in (d) using initial (solid line) and instantaneous (dashed line) measurables. Symbol size increases with the time-course of the reaction. (d) Symbols and error bars: means and standard deviations of the initial reaction rates (v_0) and instantaneous reaction rates (v_i) represented as a function of S_0 (open symbols) and S_i (closed symbols), respectively. Lines: using the MM-like equation to fit v_0 vs. S_0 data (solid line, $K_m = 55.8 \pm 9.3$ μM and $V = 44.1 \pm 2.3$ μM/h, $R^2 = 0.9929$) and v_i vs. S_i data (dashed line, $K_m = 26.9 \pm 7.2$ μM and $V = 52.6 \pm 3.4$ μM/h, $R^2 = 0.9839$). The LM test is not passed because the individual trends in (c) fail to converge into a single overall straight line.

fundamental characterization of the inhibition mechanism to future research. This model system is useful to illustrate how the presence in subnanomolar amounts (0.40 nM) of a given compound might be revealed by characteristic kinetic signatures left in LM curves. The sigmoid-shaped onset of the α-thrombin progress curves (Fig. 9a) is admissible under conditions of $S_0 \leq E_0$ that do not apply here [34]. Once again, the ill-defined initial rates can admittedly result from the gradual stabilization of the experimental conditions and not necessarily from the presence of enzyme modifiers. Yet, unlike what was observed for capase-3, the first LM representation (Fig. 9b) suggests that stabilization periods much longer than 10 min are required for the emergence of negatively-sloped LM curves. Even admitting a stabilization period of 30 min in the second LM representation (Fig. 9c), no superimposable trend is clearly defined by the individual curves obtained at the different S_0 conditions. This means that, in the case of α-thrombin, imperfect temperature control during the initial reaction phases cannot be used to explain the inconsistent LM curves obtained afterwards. Taken together, the long initial periods evidencing positive LM slopes and the persisting lack of a well-defined trend common to the different S_0 conditions indicate possible deviations from the basic Briggs-Haldane

mechanism. After dismissing the hypothesis of enzyme inactivation (which can be done using the calibration curve test), the presence of high-affinity enzyme modifiers is a strong possibility to be considered even when their action is through a direct inhibition mechanism. In fact, rate equations containing squared concentration terms are not exclusive of hyperbolic modifiers but are also expected for tight-binding linear inhibitors occurring at concentrations in the order of magnitude of E_0 or lower [48–50]. For this reason, unsuspected contaminants that are also tight-binding modifiers will have their effects uncovered by representing the measured progress curves in LM coordinates. Although the saturation plots obtained using initial (index 0) or instantaneous (index *i*) variables correspond to typical MM curves (Fig. 9d), the fitted parameters are, in both cases, of ambiguous physical meaning. The v_0 vs. S_0 analysis (solid lines in Fig. 9b and Fig. 9c) clearly does not pass the LM test, as the theoretical LM curve (solid line in Fig. 9c) fails to intercept the experimental LM curves. When instantaneous measurables are analyzed (dashed lines in Fig. 9c and Fig. 9d), the theoretical LM curve is able to intercept, at least in part, the experimental results obtained for each S_0 condition (Fig. 9c); even so, the α-thrombin enzymatic assay is considered non-compliant with the LM prerequisites because the individual LM time-course trends (indicated by symbol size increase in Fig. 9c) are divergent from the overall straight line suggested by the theoretical LM curve (dashed line in Fig. 9c). This didactic example serves to demonstrate that assay interferences cannot be diagnosed solely based on the quality of numerical adjustments to the MM equation. In contrast, kinetic effects caused by very small amounts of either linear or hyperbolic inhibitors can be detected by the LM test.

4.5. The LM test as a routine quality check

The LM test is suitable for routine use in enzymatic assay validation and to decide which optimization steps should be taken in order to improve reproducibility and accuracy. As summarized in Fig. 10, its application is based on the LM representations of reaction progress curves obtained for a fixed value of E_0 and varying S_0. First, the coordinates $\Delta P/\Delta t$ and $-\ln(1 - \Delta P/\Delta P_\infty)/\Delta t$ are computed using the beginning of the measurements ($t_i = 0$ min) as initial condition for identifying the initial period of stabilization of reaction conditions. If the obtained LM curves are negatively-sloped straight lines and tend to superimpose since the beginning of the reaction, the test is passed. If evident deviations from the ideal trend are found to occur, new coordinates must be computed using as initial reference any instant subsequent to the period of stabilization ($t_i > 0$ min). If the LM test is still not passed, the presence of enzyme inactivation can be tested using the calibration-curve test. Some assay interferences can be minimized by increasing the concentration and/or purity of the enzyme; the presence of unspecific assay interferences must also be checked here. This process can be repeated iteratively until the enzymatic assay is fully optimized. It should also be noted that repeated failure to optimize the enzymatic assay using this method can indicate the presence of a kinetic mechanism that deviates from that of Briggs-Haldane. Further kinetic studies using complementing methodologies should be considered in such case. Next, we present additional practical guidelines to be considered during the systematization of the new method.

More complete information is provided by the LM test when full progress curves are measured. Note, for example, that the $\Delta P/\Delta t$ coordinate does not change during the whole initial period of constant velocity. If, in a limit case, all points are collected within constant velocity timeframes, no individual trends will be defined for each substrate concentration and the result of the test will be solely dictated by the linearity of the overall trend. Time-dependent changes in enzymatic activity can thus be missed when only a part of the reactions is analyzed. Letting the reaction proceed until its end also allows identifying the differences between P_∞ and S_0 values upon which the calibration-
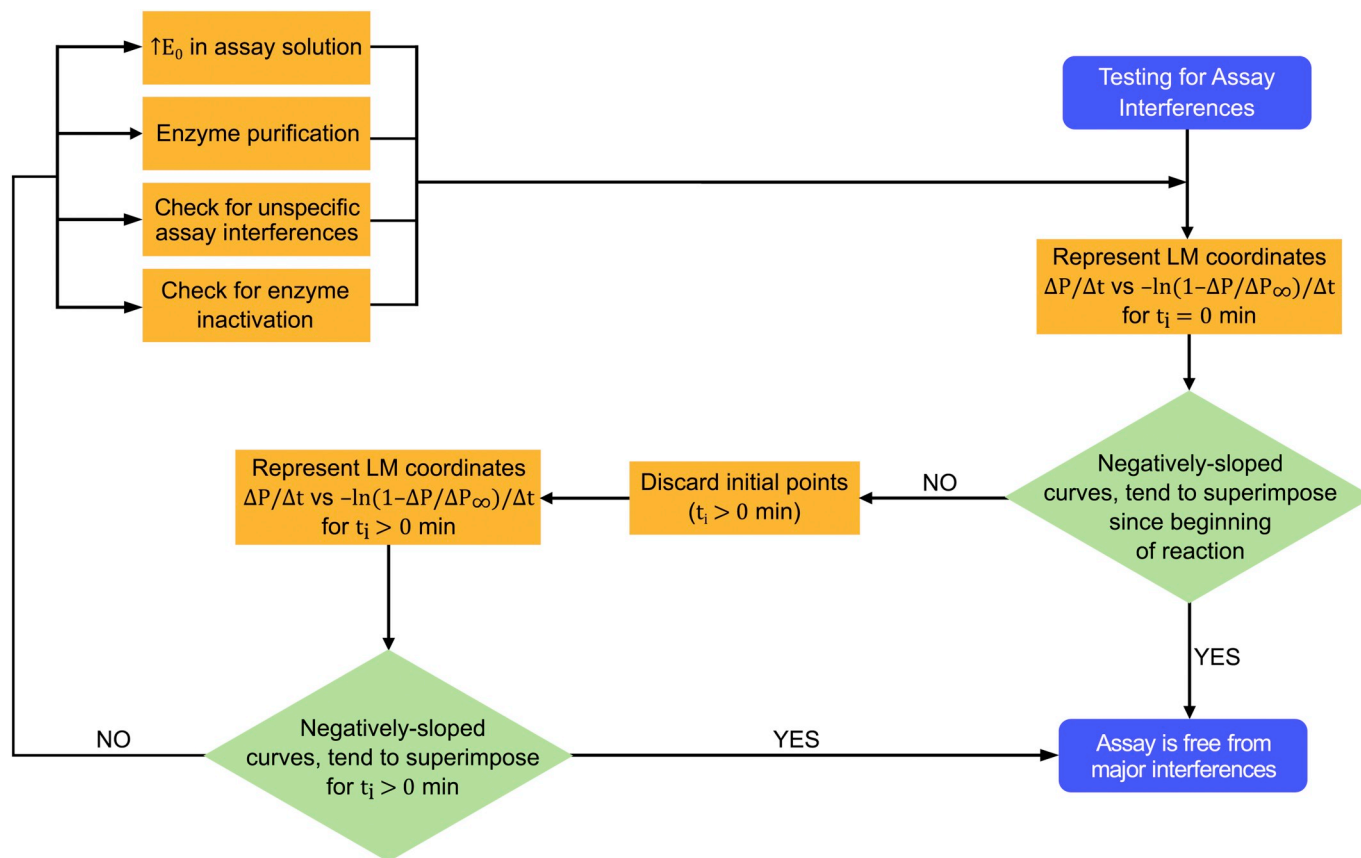
Fig. 10. Flowchart depicting the main steps of the LM test for the identification of assay interferences.

curve test is based. Although less sensitive than the LM test, the calibration-curve test is specific for enzyme inactivation and, for this reason, is indicated for the preliminary assessments of this type of interference. Nonetheless, as shown for the case of α-thrombin, reaction progress curves that reach a final plateau indicating reaction completion are not mandatory for the application of the LM test.

Small errors in reagent handling give rise to differences between the values of P_∞ and S_0 that are only evident at the end of the reaction. Such unspecific interferences are detected by the LM test even if the final product concentrations are not known, and S_0 values have to be used instead of P_∞ to compute the $-\ln(1 - \Delta P/\Delta P_\infty)/\Delta t$ coordinate. In the numerical example given in the Appendix (Fig. A2), a random error of 5% in the value of S_0 generates, since the beginning of the reaction, a clear deviation of the biased LM curve relatively to the overall trend defined by the other LM curves. As the reaction progresses in time, the differences become more pronounced and even the initial linearity is lost. A consequence of the Walker and Schmidt-type linearization [30,35] adopted by the LM equation, this high responsiveness to random experimental errors is helpful for controlling the validity of each reaction rate measurement.

5. Conclusions

A new method to identify assay interferences is proposed based on a modified version of the integrated MM equation. To pass the so called "LM test", progress curves measured at different substrate concentrations and represented in linearized $\Delta P/\Delta t$ vs. $-\ln(1 - \Delta P/\Delta P_\infty)/\Delta t$ coordinates should superimpose in a single, negatively-sloped straight line. The proposal of this new method follows from the recently

obtained closed-form solution of the Briggs-Haldane reaction mechanism [34,36]. Some of the modifications now introduced to the integrated MM equation allow time-course kinetic analysis to be carried out in the range of conditions commonly adopted for steady-state analysis ($E_0 \ll S_0 + K_m$). The illustrative examples of enzymatic reactions catalyzed by procaspase-3, caspase-3 and α-thrombin highlight different aspects that can stealthily influence the quality of enzymology data. Initial rate measurements during the catalysis of Ac-DEVD-AMC by procaspase-3 in yeast cell extracts are strongly affected by progressive enzyme inactivation, promptly detected by the LM test independently of whether such suspicion exists *a priori* or not. The Selwyn test, a reference method to identify enzyme inactivation [12,51], is less sensitive than the LM test and requires additional experiments whenever enzyme inactivation is somehow suspected to occur. The catalysis of Ac-DEVD-AMC by purified caspase-3 was used to demonstrate that non-conformities in the first LM representation are a possible indication that the experimental conditions were not yet stabilized at the beginning of the measurements. In fact, the LM representation obtained after discarding the initial stabilization period validated the caspase-3 assay, which was then used to determine unbiased MM parameters based on instantaneous values of substrate concentration and reaction rate. Finally, the inhibition of α-thrombin by subnanomolar concentrations of a synthetic anticoagulant showed the interest of the LM test in amplifying subtle enzyme modifier effects. This example illustrated that high-affinity contaminants may affect enzyme kinetics in a hard to detect way unless LM plots are represented and individual LM curves are compared with the overall trend.

Because stringent criteria are adopted, nonstandard catalytic reactions (characterized by multiple active sites, multiple substrates,

product inhibition, hyperbolic inhibition, tight-binding inhibition, enzyme inactivation, etc.), or that are influenced by instrumental noise and poor automatic control will probably not pass the LM test. This fine quality control is crucial for the success of quantitative kinetic analysis since important mechanistic nuances "may play a subordinated role with respect to even modest mistakes in reagent handling, (...) instrumental noise and others" [52]. In line with current initiatives to improve enzymology data reporting [53,54], this new method is expected to contribute in improving the reproducibility of kinetic data, thus increasing the impact of fundamental and applied research in fields such as enzyme engineering, systems biology and drug discovery.
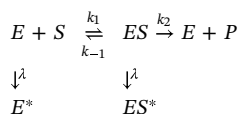
Acknowledgements

Appendix

A.1. Irreversible enzyme inactivation - numeric solutions

The Briggs-Haldane reaction scheme comprises the binding of substrate (S) to free enzyme (E) to give rise to the enzyme-substrate complex (ES), from which the catalytic product (P) is formed and released, thereby regenerating the free enzyme. Irreversible enzyme inactivation can be accounted for in this scheme by considering that free and bound enzyme decay irreversibly into the inactive forms (E^* and ES^*). For simplicity we will assume that both processes are well described by the same first-order rate constant (λ):

$$E + S \underset{k_{-1}}{\overset{k_1}{\rightleftharpoons}} ES \overset{k_2}{\to} E + P$$
$$\downarrow^\lambda \qquad\qquad \downarrow^\lambda$$
$$E^* \qquad\qquad ES^*$$

This reaction scheme is mathematically described by the following system of first-order differential equations:

$$\frac{d[S]}{dt} = k_{-1}[ES] - k_1[E][S] \tag{A.1a}$$

$$\frac{d[ES]}{dt} = k_1[E][S] - (k_{-1} + k_2 + \lambda)[ES] \tag{A.1b}$$

$$\frac{d[E]}{dt} = (k_{-1} + k_2)[ES] - k_1[E][S] - \lambda[E] \tag{A.1c}$$

$$\frac{d[P]}{dt} = k_2[ES] \tag{A.1d}$$

subject to the initial conditions $([S],[ES],[E],[P]) = (S_0, 0, E_0, 0)$ and to the mass conservation laws $E_0 = [E] + [ES] + [E^*] + [ES^*]$ and $S_0 = [S] + [ES] + [P]$. The concentrations of the different species can be normalized by the Michaelis constant $K_m = (k_{-1} + k_2)/k_1$ as $s = [S]/K_m$, $c = [ES]/K_m$, $e = [E]/K_m$ and $p = [P]/K_m$, and expressed as a function of the modified timescale $\theta = k_2 t$:

$$\left(1 - \frac{K_S}{K_m}\right)\frac{ds}{d\theta} = \frac{K_S}{K_m}c - es \tag{A.2a}$$

$$\left(1 - \frac{K_S}{K_m}\right)\frac{dc}{d\theta} = es - c(1 + \Lambda) \tag{A.2b}$$

$$\left(1 - \frac{K_S}{K_m}\right)\frac{de}{d\theta} = c - es - \Lambda e \tag{A.2c}$$

$$\frac{dp}{d\theta} = c \tag{A.2d}$$

where $K_S = k_{-1}/k_1$ is the dissociation constant of the enzyme-substrate complex, and Λ is a normalization of λ:

$$\Lambda = \left(1 - \frac{K_S}{K_m}\right)\tau\lambda e_0 \tag{A.3}$$

The system of ordinary differential equations comprising Eqs. (A.2a)–(A.2d) was numerically solved using the *ode15s* solver of Mathworks®
MATLAB R2018a (Natick, MA, USA) for the sets of simulation parameters summarized in Tables A1, A3, and A4.

A.2. Irreversible enzyme inactivation - approximate analytical solution

The instantaneous concentration of total active enzyme (E_a) is given by the sum of active enzyme in its free (E) and bound state (ES). Since both
forms are assumed to inactivate at the same rate, the evolution of E_a over time assumes the form of an exponential decay function:

$$E_a = E_0 e^{-\lambda t} \tag{A.4}$$

For sufficiently high values of initial substrate concentration S_0, Pinto, et al. [34] showed that the reaction rate equation (Eq. (A.1d)) can be
rewritten as:

$$\frac{\mathrm{d}[P]}{\mathrm{d}t} = E_a \frac{S_0 - P}{S_0 - P + K_m} \tag{A.5}$$

After replacing the time-dependent definition of E_a (Eq. (A.4)), the analytical integration of A.5 gives the evolution of $[P]$ as a function of the time
t in the presence of enzyme inactivation:

$$\frac{[P]}{K_m} - \ln\left(\frac{S_0 - P}{S_0}\right) = \frac{1}{\tau\lambda}(1 - e^{-\lambda t}) \tag{A.6}$$

with $\tau = K_m/(k_2 E_0)$. The limit of Eq. (A.6) for $t \to +\infty$ defines the final concentration of obtained product P_∞ as a function of S_0:

$$\frac{P_\infty}{K_m} - \ln\left(\frac{S_0 - P_\infty}{S_0}\right) = \frac{1}{\tau\lambda} \tag{A.7}$$

The Lambert ω function is a built-in function in mathematical software that satisfies the transcendental equation $\omega(x)e^{\omega(x)} = x$. It is used to
express Eqs. (A.6) and (A.7) as closed-form solutions, solving for $[P]$ (Eq. (A.8)) and P_∞ (Eq. (A.9)):

$$[P] = S_0 - K_m \omega\left[\frac{S_0}{K_m}\exp\left(\frac{S_0}{K_m} - \frac{1}{\tau\lambda}(1 - \exp(-\lambda t))\right)\right] \tag{A.8}$$

$$P_\infty = S_0 - K_m \omega\left[\frac{S_0}{K_m}\exp\left(\frac{S_0}{K_m} - \frac{1}{\tau\lambda}\right)\right] \tag{A.9}$$

Eq. (A.9) was used to simulate P_∞/K_m vs S_0/K_m curves for the sets of simulation parameters summarized in Table A2.

A.3. Reaction rate analysis

Initial reaction rates (v_0) of progress curves for varying substrate concentrations were obtained by linear regression and analyzed to determine
kinetic parameters K_m and $V = k_2 E_0$. Data were fitted to the MM equation (Eq. (A.10)) by the non-linear least-squares method.

$$v_0 = \frac{VS_0}{S_0 + K_m} \tag{A.10}$$

For procaspase-3 data, initial time intervals with approximate linear behavior were chosen for v_0 determination (Table A5). For recombinant
caspase-3 and α-thrombin data, initial velocity and instantaneous velocity values (v_0 and v_i, respectively) were determined. The selected time
intervals used in each case are listed in Table A5. Instantaneous substrate concentrations S_i were determined for the median points of the intervals
chosen for v_i determination. Non-linear least-squares fitting of v_i vs S_i was performed using the MM-like equation described by Pinto, et al. [34]:

$$v_i = \frac{VS_i}{S_i + K_m} \tag{A.11}$$

The fitted coefficients are presented with standard errors for 95% confidence level as estimated by the *fit* and *fitlm* functions of Mathworks®
MATLAB R2018a (Natick, MA, USA).

A.4. Figures
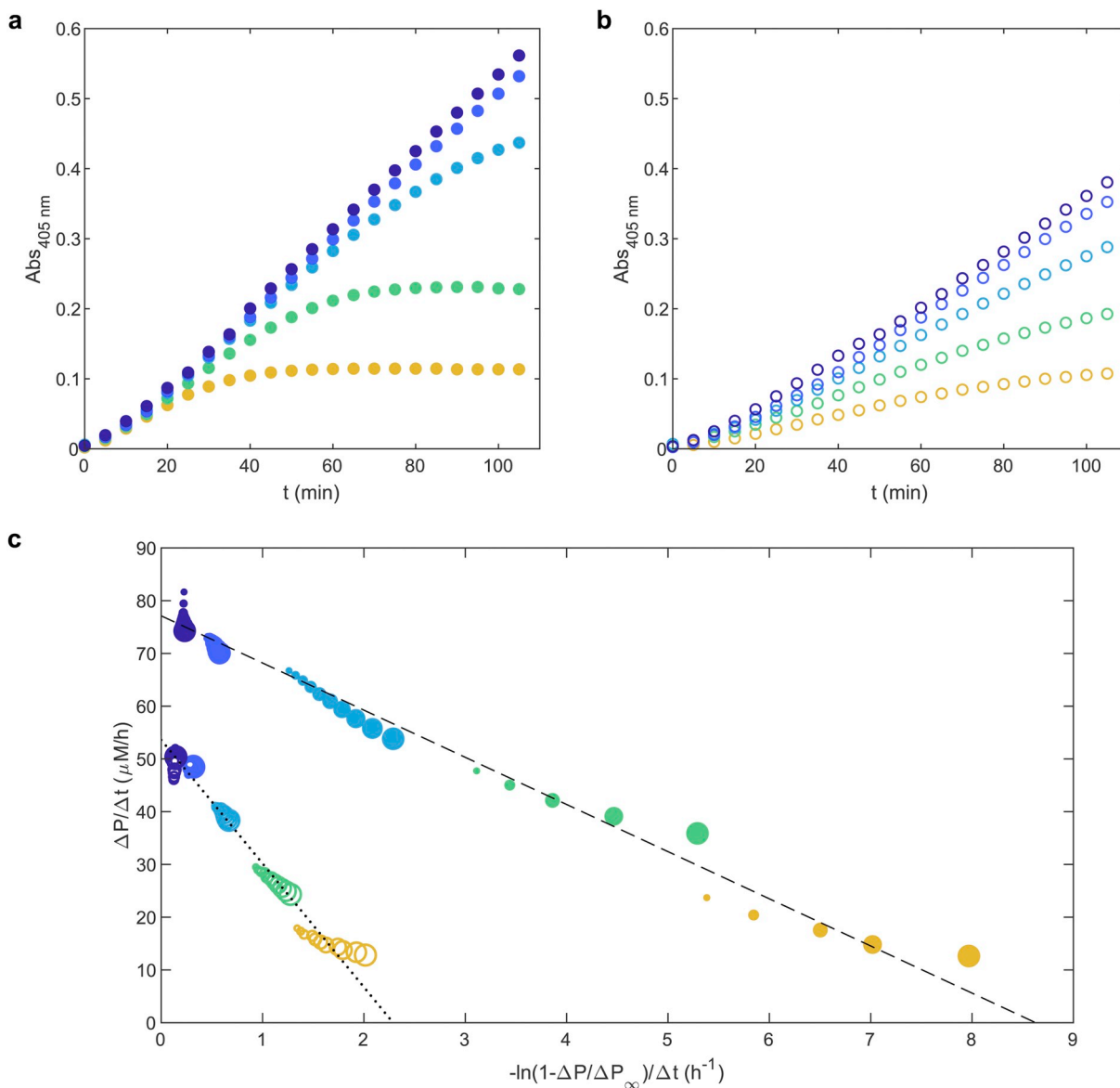
**Fig. A1.** The presence of subnanomolar amounts (0.40 nM) of a synthetic variant of an anticoagulant produced by *D. andersoni* inhibits the catalysis of Tos-Gly-Pro-Arg-p-NA by 0.15 nM α-thrombin. (a and b) Absorbance (Abs_{405nm}) increase measured in the absence (a) and presence (b) of inhibitor for substrate concentrations of (from top to bottom) 400, 200, 100, 50 and 25 μM. (c) The same progress curves are represented according to the linearization method (LM) scale using $t_i = 30$ min (color-coded as in Figs. A1a and A1b). Symbol size increases according to the time-course of the reaction. Lines: representation of the theoretical LM equation (Eq. (2)) using $K_m^{app} = 8.94 \pm 0.17$ μM and $V^{app} = 77.1 \pm 0.5$ μM/h (dashed line, $R^2 = 0.9838$) and $K_m^{app} = 23.4 \pm 0.5$ μM and $V^{app} = 53.6 \pm 0.4$ μM/h (dotted line, $R^2 = 0.9730$).

a

b
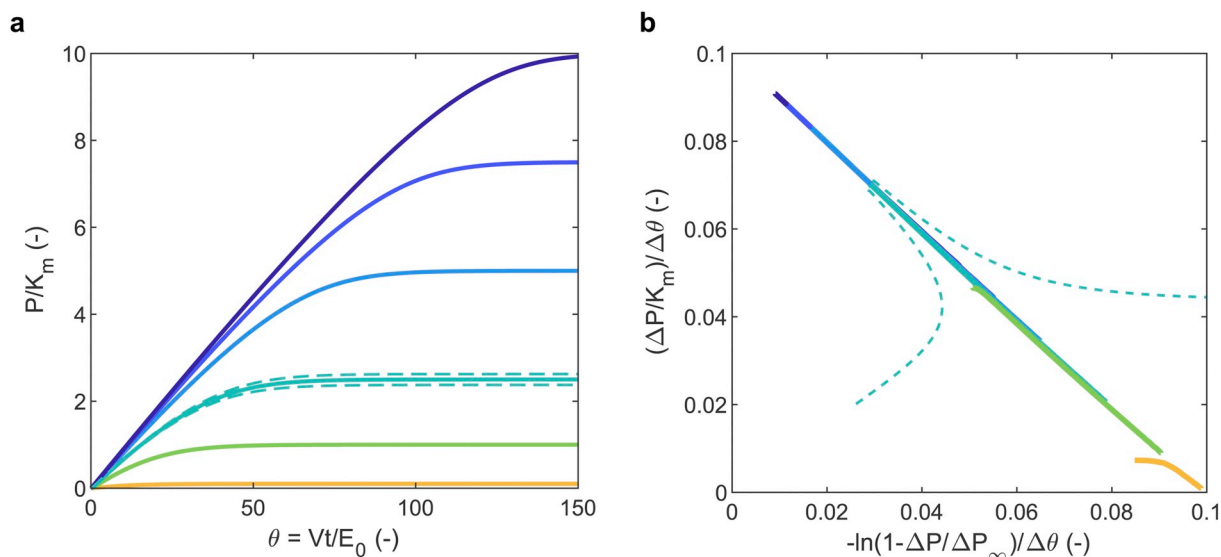
Fig. A2. Small errors in reagent handling can be detected by the LM test. (a) Solid lines: theoretical progress curves calculated as described in Fig. 2a for S_0/K_m values of (from top to bottom) 10, 7.5, 5, 2.5, 1, 0.1. Dashed lines: theoretical progress curves simulated for a random error of $\pm$ 5% in the value of $S_0/K_m = 2.5$. (b) Lines: the same progress curves are represented in the LM scale using $t_i = 0$, and $P_\infty = S_0$. A clear deviation of the biased LM curves relatively to the overall trend can be identified since the beginning of the reaction.

A.5. Tables

Table A1
Model parameters used for simulation of reaction progress curves and LM curves presented in Fig. 2.

$e_0 = E_0/K_m \ (-)$	$S_0/K_m \ (-)$	$K_s/K_m \ (-)$	$\lambda/k_2 \ (-)$	$\tau\lambda = (\lambda/k_2)(1/e_0) \ (-)$
0.1	0.1	0	0	0
	1			
	2.5			
	5			
	7.5			
	10			

Table A2
Model parameters used for simulation of P_∞/K_m vs S_0/K_m curves presented in Fig. 6a.

$e_0 = E_0/K_m \ (-)$	$S_0/K_m \ (-)$	$K_s/K_m \ (-)$	$\lambda/k_2 \ (-)$	$\tau\lambda = (\lambda/k_2)(1/e_0) \ (-)$
10^{-3}	[0,10]	1	0	0
			10^{-6}	10^{-3}
			10^{-5}	0.01
			10^{-4}	0.1[a]
			1.5×10^{-4}	0.15
			2.5×10^{-4}	0.25
			5×10^{-4}	0.5
			1×10^{-3}	1
			5×10^{-3}	5

[a] Inactivation effects are poorly detected by the calibration-curve test for reference values of $\tau\lambda < 0.1$.

Table A3
Model parameters used for simulation of reaction progress curves presented in Fig. 6b.

$e_0 = E_0/K_m \ (-)$	$S_0/K_m \ (-)$	$K_s/K_m \ (-)$	$\lambda/k_2 \ (-)$	$\tau\lambda = (\lambda/k_2)(1/e_0) \ (-)$
10^{-3}	5	1	10^{-4}	0.1[a]
1.3×10^{-3}				0.08
2×10^{-3}				0.05
4×10^{-3}				0.03
0.01				0.01
0.1				10^{-3}

[a] Inactivation effects are poorly detected by the Selwyn test for reference values of $\tau\lambda < 0.1$.

Table A4

Model parameters used for simulation of LM curves presented in Fig. 6c.

$e_0 = E_0/K_m$ $(-)$	S_0/K_m $(-)$	K_s/K_m $(-)$	λ/k_2 $(-)$	$\tau\lambda = (\lambda/k_2)(1/e_0)$ $(-)$
10^{-3}	0.01	1	10^{-4}	0.1[a]
	0.1			
	0.5			
	0.75			
	1			
	1.5			
	2.5			
	5			
	10			

[a] Inactivation effects are still detected by the LM test for a reference value of $\tau\lambda = 0.1$.

Table A5

Time intervals employed for determination of initial reaction velocity v_0 and instantaneous reaction velocity v_i by linear regression for procaspase-3, purified caspase-3 and α-thrombin enzymatic assays.

Procaspase-3	S_0 (μM)	3.125	6.25	12.5	25	50	100	150	200	300
	t_{int} (h) for v_0	[0,0.05]	[0,0.05]	[0,0.07]	[0,0.125]	[0,0.25]	[0,0.5]	[0,0.75]	[0,1]	[0,2]

Caspase-3	S_0 (μM)	3.125	6.25	12.5	25	50
	t_{int} (h) for v_0	[0,0.15]	[0,0.15]	[0,0.15]	[0,0.15]	[0,0.15]
	t_{int} (h) for v_i	[0.15,0.20]	[0.15,0.20]	[0.15,0.25]	[0.15,0.25]	[0.15,0.30]
α-Thrombin $I = 0.40$ nM	S_0 (μM)	25	50	100	200	400
	t_{int} (min) for v_0	[0, 30]	[0, 30]	[0, 30]	[0, 30]	[0, 30]
	t_{int} (min) for v_i	[30, 60]	[30, 60]	[30, 60]	[30, 60]	[30, 60]

References

[1] G.A. Holdgate, T.D. Meek, R.L. Grimley, Mechanistic enzymology in drug discovery: a fresh perspective, Nat. Rev. Drug Discov. 17 (2018) 115–132.

[2] M. Rask-Andersen, S. Masuram, H.B. Schiöth, The druggable genome: evaluation of drug targets in clinical trials suggests major shifts in molecular class and indication, Annu. Rev. Pharmacol. Toxicol. 54 (2014) 9–26.

[3] N. Thorne, D.S. Auld, J. Inglese, Apparent activity in high-throughput screening: origins of compound-dependent assay interference, Curr. Opin. Chem. Biol. 14 (2010) 315–324.

[4] C. Aldrich, C. Bertozzi, G.I. Georg, L. Kiessling, C. Lindsley, D. Liotta, K.M. Merz, A. Schepartz, S. Wang, The ecstasy and agony of assay interference compounds, ACS Cent. Sci. 3 (2017) 143–147.

[5] T.F.T. Rexer, A. Schildbach, J. Klapproth, A. Schierhorn, R. Mahour, M. Pietzsch, E. Rapp, U. Reichl, One pot synthesis of GDP-mannose by a multi-enzyme cascade for enzymatic assembly of lipid-linked oligosaccharides, Biotechnol. Bioeng. 115 (2018) 192–205.

[6] K. Yu, S. Hu, J. Huang, L.-H. Mei, A high-throughput colorimetric assay to measure the activity of glutamate decarboxylase, Enzym. Microb. Technol. 49 (2011) 272–276.

[7] W. Cao, E.M. De La Cruz, Quantitative full time course analysis of nonlinear enzyme cycling kinetics, Sci. Rep. 3 (2013) 2658.

[8] B.K. Shoichet, Screening in a spirit haunted world, Drug Discov. Today 11 (2006) 607–615.

[9] J.-H. Grosch, D. Wagner, N. Knaup, T. Keil, A.C. Spieß, Influence of the experimental setup on the determination of enzyme kinetic parameters, Biotechnol. Prog. 33 (2017) 87–95.

[10] F. Gielen, L. van Vliet, B.T. Koprowski, S.R.A. Devenish, M. Fischlechner, J.B. Edel, X. Niu, A.J. deMello, F. Hollfelder, A fully unsupervised compartment-on-demand platform for precise nanoliter assays of time-dependent steady-state enzyme kinetics and inhibition, Anal. Chem. 85 (2013) 4761–4769.

[11] A. Cornish-Bowden, One hundred years of Michaelis–Menten kinetics, Perspect. Sci. 4 (2015) 3–9.

[12] M.J. Selwyn, A simple test for inactivation of an enzyme during assay, Biochim. Biophys. Acta 105 (1965) 193–195.

[13] S. Schnell, S.M. Hanson, A test for measuring the effects of enzyme inactivation, Biophys. Chem. 125 (2007) 269–274.

[14] B.Y. Feng, B.K. Shoichet, A detergent-based assay for the detection of promiscuous inhibitors, Nat. Protoc. 1 (2006) 550–553.

[15] N.D. Rawlings, A.J. Barrett, P.D. Thomas, X. Huang, A. Bateman, R.D. Finn, The MEROPS database of proteolytic enzymes, their substrates and inhibitors in 2017 and a comparison with peptidases in the PANTHER database, Nucleic Acids Res. 46 (2018) D624–D632.

[16] K.M. Boatright, G.S. Salvesen, Mechanisms of caspase activation, Curr. Opin. Cell Biol. 15 (2003) 725–731.

[17] J.T.B. Crawley, S. Zanardelli, C.K.N.K. Chion, D.A. Lane, The central role of thrombin in hemostasis, J. Thromb. Haemost. 5 (2007) 95–101.

[18] M.Á. Corral-Rodríguez, S. Macedo-Ribeiro, P.J. Barbosa Pereira, P. Fuentes-Prior, Tick-derived Kunitz-type inhibitors as antihemostatic factors, Insect Biochem. Mol. Biol. 39 (2009) 579–595.

[19] M.Á. Corral-Rodríguez, S. Macedo-Ribeiro, P.J. Barbosa Pereira, P. Fuentes-Prior, Leech-derived thrombin inhibitors: from structures to mechanisms to clinical applications, J. Med. Chem. 53 (2010) 3847–3861.

[20] F.L. Ware, M.R. Luck, Evolution of salivary secretions in haematophagous animals, Biosci. Horizons. 10 (2017) hzw015.

[21] L.F. Parizi, A. Ali, L. Tirloni, D.P. Oldiges, G.A. Sabadin, M.L. Coutinho, A. Seixas, C. Logullo, C. Termignoni, I. da Silva Vaz Jr, Peptidase inhibitors in tick physiology, Med. Vet. Entomol. 32 (2018) 129–144.

[22] I.M. Francischetti, A. Sa-Nunes, B.J. Mans, I.M. Santos, J.M. Ribeiro, The role of saliva in tick feeding, Front. Biosci. (Landmark Ed) 14 (2009) 2051–2088.

[23] Watson, E. E., Ripoll-Rozada, J., Lee, A. C., Wu, M. C. L., Franck, C., Pasch, T., Premdjee, B., Sayers, J., Pinto, M. F., Martins, P. M., Jackson, S. P., Pereira, P. J. B. and Payne, R. J. (2019). Rapid Assembly of a Library of Anticoagulant Sulfoproteins. (In Press). Doi: 10.1073/pnas.1905177116.

[24] C. Pereira, V. Lopes-Rodrigues, I. Coutinho, M.P. Neves, R.T. Lima, M. Pinto, H. Cidade, M.H. Vasconcelos, L. Saraiva, Potential small-molecule activators of caspase-7 identified using yeast-based caspase-3 and -7 screening assays, Eur. J. Pharm. Sci. 54 (2014) 8–16.

[25] P.M.C. Gloria, I. Coutinho, L.M. Goncalves, C. Baptista, J. Soares, A.S. Newton, R. Moreira, L. Saraiva, M.M. Santos, Aspartic vinyl sulfones: inhibitors of a caspase-3-dependent pathway, Eur. J. Med. Chem. 46 (2011) 2141–2146.

[26] D. Boucher, C. Duclos, J.-B. Denault, Caspases, paracaspases and metacaspases: methods and protocols, Methods Mol Biol, Humana Press, 2014, pp. 3–39.

[27] R.E. Thompson, X. Liu, J. Ripoll-Rozada, N. Alonso-García, B.L. Parker, P.J.B. Pereira, R.J. Payne, Tyrosine sulfation modulates activity of tick-derived thrombin inhibitors, Nat. Chem. 9 (2017) 909–917.

[28] S. Schnell, C. Mendoza, Closed form solution for time-dependent enzyme kinetics, J. Theor. Biol. 187 (1997) 207–212.

[29] R.G. Duggleby, Quantitative analysis of the time courses of enzyme-catalyzed reactions, Methods 24 (2001) 168–174.

[30] B.A. Orsi, K.F. Tipton, Kinetic analysis of progress curves, Methods Enzymol. 63 (1979) 159–183.

[31] J. Eicher, J. Snoep, J. Rohwer, Determining enzyme kinetics for systems biology with nuclear magnetic resonance spectroscopy, Metabolites 2 (2012) 818–843.

[32] W. Stroberg, S. Schnell, On the estimation errors of K_M and V from time-course experiments using the Michaelis–Menten equation, Biophys. Chem. 219 (2016) 17–27.

[33] S.M. Hanson, S. Schnell, Reactant stationary approximation in enzyme kinetics, J. Phys. Chem. A 112 (2008) 8654–8658.

[34] M.F. Pinto, B.N. Estevinho, R. Crespo, F.A. Rocha, A.M. Damas, P.M. Martins, Enzyme kinetics: the whole picture reveals hidden meanings, FEBS J. 282 (2015) 2309–2316.

[35] A.C. Walker, C.L.A. Schmidt, Studies on histidase, Arch. Biochem. Biophys. 5 (1944) 445–467.

[36] M.F. Pinto, P.M. Martins, In search of lost time constants and of non-Michaelis-

Menten parameters, Perspect. Sci. 9 (2016) 8–16.

[37] G.A. Fleisher, Curve fitting of enzymatic reactions based on the Michaelis—Menten equation[1], J. Am. Chem. Soc. 75 (1953) 4487–4490.

[38] G.E. Briggs, J.B.S. Haldane, A note on the kinetics of enzyme action, Biochem. J. 19 (1925) 338–339.

[39] H. Bisswanger, Enzyme assays, Perspect. Sci. 1 (2014) 41–55.

[40] Q. Tang, T.S. Leyh, Precise, facile initial rate measurements, J. Phys. Chem. B 114 (2010) 16131–16136.

[41] K. Bose, C. Pop, B. Feeney, A.C. Clark, An uncleavable procaspase-3 mutant has a lower catalytic efficiency but an active site similar to that of mature caspase-3, Biochemistry 42 (2003) 12298–12310.

[42] A. Cornish-Bowden, The use of the direct linear plot for determining initial velocities, Biochem. J. 149 (1975) 305–312.

[43] A. Cornish-Bowden, Fundamentals of Enzyme Kinetics, 4th edn, Wiley-Blackwell, Weinheim, Germany, 2012 p. 44.

[44] S. Matosevic, N. Szita, F. Baganz, Fundamentals and applications of immobilized microfluidic enzymatic reactors, J. Chem. Technol. Biotechnol. 86 (2011) 325–334.

[45] T.H. Sørensen, N. Cruys-Bagger, M.S. Windahl, S.F. Badino, K. Borch, P. Westh, Temperature effects on kinetic parameters and substrate affinity of Cel7A cellobiohydrolases, J. Biol. Chem. 290 (36) (2015) 22193–22202.

[46] S. Schnell, Validity of the Michaelis-Menten equation – steady-state or reactant stationary assumption: that is the question, FEBS J. 281 (2014) 464–472.

[47] J. Botts, M. Morales, Analytical description of the effects of modifiers and of enzyme multivalency upon the steady state catalyzed reaction rate, Trans. Faraday Soc. 49 (1953) 696–707.

[48] P.J.F. Henderson, Steady-state enzyme kinetics with high-affinity substrates or inhibitors. A statistical treatment of dose–response curves, Biochem. J. 135 (1973) 101–107.

[49] J.F. Morrison, Kinetics of the reversible inhibition of enzyme-catalysed reactions by tight-binding inhibitors, Biochim. Biophys. Acta 185 (1969) 269–286.

[50] S.E. Szedlacsek, R.G. Duggleby, [6] Kinetics of slow and tight-binding inhibitors, Methods Enzymol, 249 Academic Press, 1995, pp. 144–180.

[51] S. Ben Halima, S. Mishra, K. Raja, P. Muruga, M. Willem, A. Baici, K. Simons, O. Brüstle, P. Koch, C. Haass, A. Caflisch, L. Rajendran, Specific inhibition of β-secretase processing of the Alzheimer disease amyloid precursor protein, Cell Rep. 14 (2016) 2127–2141.

[52] A. Baici, Kinetics of Enzyme-Modifier Interactions, 1st edn, Springer, 2015 p. 108.

[53] N. Swainston, A. Baici, B.M. Bakker, A. Cornish-Bowden, P.F. Fitzpatrick, P. Halling, T.S. Leyh, C. O'Donovan, F.M. Raushel, U. Reschel, J.M. Rohwer, S. Schnell, D. Schomburg, K.F. Tipton, M.-D. Tsai, H.V. Westerhoff, U. Wittig, R. Wohlgemuth, C. Kettner, STRENDA DB: enabling the validation and sharing of enzyme kinetics data, FEBS J. 285 (2018) 2193–2204.

[54] P.C.F. Buchholz, C. Vogel, W. Reusch, M. Pohl, D. Rother, A.C. Spieß, J. Pleiss, BioCatNet: a database system for the integration of enzyme sequences and biocatalytic experiments, ChemBioChem. 17 (2016) 2093–2098.